Redox Chemistry of (1,4,7-Tris(4-*tert*-butyl-2-mercaptobenzyl)-1,4,7-triazacyclononane)ruthenium(III), [Ru^{III}L]: Synthesis and Characterization of $[Ru^{II}_2(L-L)](BPh_4)_4 \cdot 10CH_3CN$ and $[LRuRuRuL](PF_6)_2 \cdot H_2O$

Belén Albela, Eberhard Bothe, Oliver Brosch, Katsura Mochizuki, Thomas Weyhermüller, and Karl Wieghardt*

Max-Planck-Institut für Strahlenchemie, Stiftstrasse 34−36, D-45470 Mülheim an der Ruhr, Germany

Received June 2, 1999

The mononuclear blue complex [Ru^{III}L] (**1**) where L represents the trianion of 1,4,7-tris(4-*tert*-butyl-2-mercaptobenzyl)-1,4,7-triazacyclononane has been synthesized by the reaction of $H_3L \cdot 3HPF_6$ with $[Ru^{II}Cl_2(dmso)_4]$ in refluxing CH_3OH in the presence of air. Chemical or electrochemical oxidation of **1** generates $[Ru^{II}_2(L-L)](PF_6)_4$ (**2**), a dinuclear species containing two Ru^{II} ions and a neutral tris(disulfide) ligand L−L. The reaction of **1** with 1 equiv of $[Ru^{II}Cl_2(dmso)_4]$ produces the trinuclear species $[LRuRuRuL](PF_6)_2$ (**3**) in low yield. Complexes **2** and **3** have been structurally characterized by X-ray crystallography: $[Ru^{II}_2(L-L)](BPh_4)_4 \cdot 10CH_3CN$, $C_{194}H_{218}B_4N_{16}Ru_2S_6$, crystallizes in the monoclinic space group *C*2/c with $a = 28.734(5)$ Å, $b = 16.347(3)$ Å, $c = 37.986(7)$ Å, $\beta = 102.35(2)°$, and $Z = 4$ whereas $[LRuRuRuL](PF_6)_2 \cdot H_2O$, $C_{78}H_{110}F_{12}N_6OP_2Ru_3S_6$, crystallizes in the monoclinic space group $P2_1/n$ with $a = 18.755(4)$ Å, $b = 22.278(4)$ Å, $c = 21.920(4)$ Å, $\beta = 91.69(3)$ Å, and $Z = 4$. The electro- and spectroelectrochemistry of **1**−**3** have been studied in detail as have their electronic structures by ^{1}H NMR, EPR, UV−vis, IR, and Raman spectroscopy.

Introduction

The pendent arm macrocyclic ligand H_3L in its deprotonated trianionic form has been shown to form a wide variety of very stable mono-, di-, and trinuclear transition metal complexes (Chart 1): [M^{III}L] (M = Ga, In, V, Cr, Mn, Fe, Co)[1] and [M^{IV}L]-PF_6 (M = V^{IV}, Mn^{IV}),[1] homo- and heterodinuclear species $[LM^{II}_2Cl]$ and $[LM^1M^2Cl]$,[1c] and homo- and heterotrinuclear species $[L_2M_3]^{n+}$ and $[LM^1M^2M^1L]^{n+}$ are readily synthetically accessible;[2−4] L^{3-} represents the trianion of 1,4,7-tris(4-*tert*-butyl-2-mercaptobenzyl)-1,4,7-triazacyclononane. In mononuclear octahedral complexes, a *cis*-N_3S_3M coordination polyhedron allows one to bind a second transition metal ion at the three thiolato sulfur donor atoms in cis positions relative to each other.

In the linear trinuclear species, the central metal ion possesses an octahedral MS_6 polyhedron. This central moiety was recently shown to stabilize transition metal ions in rare high oxidation states as in $[LCo^{III}Cu^{III}Co^{III}L]^{3+}$, $[LNaRu^{IV}NaL]^0$, and $[LNaOs^{IV}NaL]^0$.[3,4] All species have a rich redox chemistry, which allows one to characterize isostructural oxidized and reduced species of a given complex and study spin-exchange phenomena as a function of the individual d^n electron configurations of given metal ions in an identical ligand matrix.[5]

Chart 1

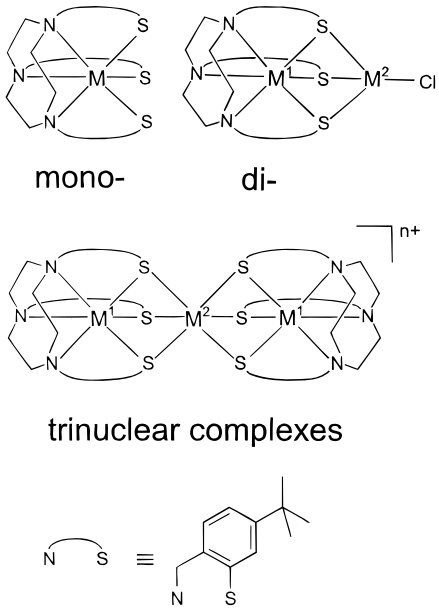

Here we report the synthesis and properties of [Ru^{III}L] (**1**), which can be chemically or electrochemically *oxidized* by two electrons per Ru ion, yielding a dinuclear species containing two *reduced* ruthenium(II) ions, $[Ru^{II}_2(L-L)](PF_6)_4$ (**2**), where

(1) Beissel, T.; Bürger, K. S.; Voigt, G.; Wieghardt, K.; Butzlaff, C.; Trautwein, A. X. *Inorg. Chem.* **1993**, *32*, 124. (b) Butzlaff, C.; Bill, E.; Meyer, W.; Winkler, H.; Trautwein, A. X.; Beissel, T.; Wieghardt, K. *Hyperfine Interact.* **1994**, *90*, 453. (c) Beissel, T.; Glaser, T.; Kesting, F.; Wieghardt, K.; Nuber, B. *Inorg. Chem.* **1996**, *35*, 3936.

(2) Beissel, T.; Birkelbach, F.; Bill, E.; Glaser T.; Kesting, F.; Krebs, C.; Weyhermüller, T.; Wieghardt, K.; Butzlaff, C.; Trautwein, A. X. *J. Am. Chem. Soc.* **1996**, *118*, 12376. (b) Glaser, T.; Kesting, F.; Beissel, T.; Bill, E.; Weyhermüller, T.; Meyer-Klaucke, W.; Wieghardt, K. *Inorg. Chem.* **1999**, *38*, 722. (c) Glaser, T.; Beissel, T.; Bill, E.; Weyhermüller, T.; Schünemann, V.; Meyer-Klaucke, W.; Trautwein, A. X.; Wieghardt, K. *J. Am. Chem. Soc.* **1999**, *121*, 2193.

(3) Krebs, C.; Glaser, T.; Bill, E.; Weyhermüller, T.; Meyer-Klaucke, W.; Wieghardt, K. *Angew. Chem., Int. Ed. Engl.* **1999**, *38*, 359.

(4) Mochizuki, K.; Kesting, F.; Weyhermüller, T.; Wieghardt, K.; Butzlaff, C.; Trautwein, A. X. *J. Chem. Soc., Chem. Commun.* **1994**, 909.

(5) Glaser, T.; Wieghardt, K. In *Spectroscopic Methods in Bioinorganic Chemistry;* Solomon, E. I., Hodgson, K. O., Eds.; ACS Symposium Series 692; American Chemical Society: Washington, DC, 1998; p 314.

10.1021/ic9906297 CCC: $18.00
Published on Web 10/13/1999

Scheme 1

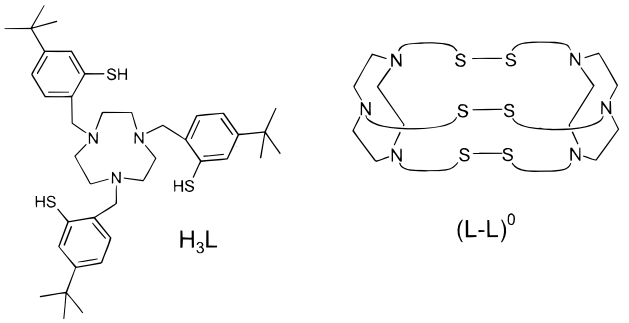

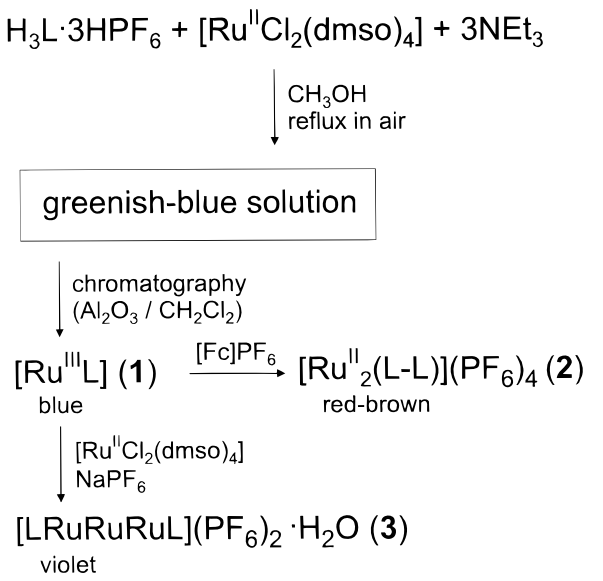

(L−L) represents the neutral dimeric, six-electron *oxidized* form of the L^{3-} ligand containing three disulfide groups (Scheme 1), eqs 1 and 2.

$$2L^{3-} \rightarrow (L-L) + 6e^- \quad (1)$$

$$2[Ru^{III}L] \rightarrow [Ru^{II}{}_2(L-L)]^{4+} + 4e^- \quad (2)$$

Furthermore, we report the synthesis and structure of the trinuclear species $[LRuRuRuL](PF_6)_2\cdot H_2O$.

Experimental Section

The ligand $H_3L\cdot 3HPF_6$ was prepared according to the published procedure[1a] for $H_3L\cdot 3HCl$ by using HPF_6 instead of HCl in the last step.

$[Ru^{III}L]\cdot H_2O$ (1). To a degassed solution of the ligand $H_3L\cdot 3HPF_6$ (1.50 g; 1.36 mmol) in CH_3OH (50 mL) were added NEt_3 (0.55 mL; 3.87 mmol) and $[Ru^{II}Cl_2(dmso)_4]$ (0.60 g; 1.24 mmol). The resulting slurry was heated to reflux under an argon blanketing atmosphere for 12 h and was then exposed to air. A blue-green microcrystalline precipitate formed, which was isolated by filtration. The crude product was purified by column chromatography from a CH_2Cl_2 solution on Al_2O_3, where the blue phase was collected. Yield: 0.58 g (55%). Anal. Calcd for $C_{39}H_{56}N_3OS_3Ru$: C, 60.04; H, 7.23; N, 5.39; S, 12.33. Found: C, 60.10; H, 7.46; N, 5.41; S, 12.63. ^{1}H NMR (400 MHz; $CDCl_3$): $\delta = -17.77$ (s, 1H), −14.56 (s, 1H), −4.02 (s, 1H), 1.2 (s, 9H), 10.93 (s, 1H), 12.05 (s, 1H), 14.13 (s, 1H); 32.67 (s, 1H), 39.03 (s, 1H).

$[Ru^{II}{}_2(L-L)](PF_6)_4$ (2). To a suspension of **1** (0.10 g; 0.13 mmol) in degassed CH_3OH (25 mL) was added ferrocenium hexafluorophosphate (0.10 g; 0.30 mmol) under argon. After the mixture was heated to reflux for 30 min, a microcrystalline red-brown precipitate formed, which was collected by filtration. Yield: 0.12 g (90%). Crystals suitable for X-ray crystallography were grown from an acetonitrile solution of **2** to which an excess of $Na[BPh_4]$ had been added. Slow evaporation of the solvent produced red-brown crystals of $[Ru^{II}{}_2(L-L)](BPh_4)_4\cdot 10CH_3CN$, which were kept in contact with the mother liquid, since the crystals were found to quickly lose solvent molecules of crystallization in dry air. A dry sample contained only two molecules of CH_3CN per dinuclear complex. Anal. Calcd for $[Ru^{II}{}_2(L-L)](BPh_4)_4\cdot 2CH_3CN$, $C_{178}H_{194}N_8S_6B_4Ru_2$: C, 74.15; H, 6.78; N, 3.89; S, 6.67. Found: C, 74.45; H, 6.84; N, 3.94; S, 6.87. ^{1}H NMR (400 MHz, CD_3CN): $\delta = 1.07$ (s, $-CH_3$, 27H), 2.2−2.70 (m, $-CH_2CH_2-$, 3H), 2.78−2.97 (m, $-CH_2CH_2$-, 9H), 4.38 (d, RCH_2N, 3H), 4.81 (d, RCH_2N, 3H), 7.04 (d, aromatic protons, 3H), 7.65 (d, aromatic protons, 3H), 7.80 (dd, aromatic protons, 3H).

$[LRuRuRuL](PF_6)_2\cdot H_2O$ (3). $[Ru^{II}Cl_2(dmso)_4]$ (0.25 g; 0.52 mmol) was added to a degassed solution of **1** (0.50 g; 0.66 mmol) in CH_3OH (150 mL). The reaction mixture was heated to reflux under an argon blanketing atmosphere for 3 h. The volume of the cooled red-violet solution was reduced to half by evaporation. Upon addition of $NaPF_6$ (1.0 g), a black precipitate formed immediately, which was collected by filtration and discarded. From the resulting solution a violet microcrystalline precipitate formed slowly upon further evaporation of solvent. The crude product dissolved in a minimum amount of CH_2Cl_2 was purified by column chromatography (Al_2O_3; 2.5% CH_3OH/CH_2Cl_2 (v/v)). After removal of the solvent, dark red microcrystals were obtained, which were recrystallized from CH_3OH solution. Single crystals were obtained from such a solution upon slow evaporation of the solvent. Yield: 0.19 g (30%). ^{1}H NMR (80 MHz, CD_3CN): $\delta =$ 0.91 (s, 27H), 3.19 (s, 12H), 3.94 (d, 3H), 5.22 (d, 3H), 7.10 (m, aromatic protons, 9H). Anal. Calcd for $C_{78}H_{110}N_6OS_6Ru_3P_2F_{12}$: C, 48.45; H, 5.73; N, 4.35; S, 9.95. Found: C, 48.46; H, 6.02; N, 4.25; S, 9.86.

Physical Measurements. Electronic spectra were recorded on a Perkin-Elmer Lambda 19 (range 220−1400 nm) or on a Hewlett-Packard HP 8452A diode array spectrophotometer (range 220−820 nm). IR and Raman spectra were recorded on a Perkin-Elmer System 2000 NIR FT-Raman (diode pumped Nd:YAG laser). Magnetic susceptibilities of powdered samples were measured in the temperature range 2−293 K on a SQUID magnetometer (MPMS, Quantum Design) in a 1 T external magnetic field. The diamagnetism of the sample was taken into account by using Pascal's constants. X-band EPR spectra of frozen solutions were measured on a Bruker ESP 300E spectrometer in a quartz cell ($d = 0.3$ mm), equipped with an Oxford Instruments ESR 910 helium-flow cryostat with an ITC 503 temperature controller. Temperature stability was 0.2 K, and the temperature gradient across the sample was estimated to be less than 0.5 K. The data were digitized by means of the data station Stelar DS-EPR (Stelar snc, Mede, Italy). We thank Dr. F. Neese (Abteilung Biologie der Universität Konstanz) for a copy of his EPR simulation program. Cyclic voltammetry, square-wave voltammetry, and coulometric experiments were performed with EG&G equipment (model 273A potentiostat/galvanostat) on solutions containing 0.10 M tetra-*n*-butylammonium hexafluorophosphate ([TBA]-PF_6) as the supporting electrolyte and $Ag/AgNO_3$ as the reference electrode. Redox potentials are referenced versus the ferrocenium/ferrocene couple (Fc^+/Fc). ^{1}H NMR spectra were recorded on a 400 MHz Bruker AMX series or on a 80 MHz Bruker WP spectrometer with the solvent as internal standard.

X-ray Crystallographic Data Collection and Refinement of the Structures. Reddish brown single crystals of **2** and **3** were mounted in sealed glass capillaries. Crystallographic data of the compounds are listed in Table 1. Cell constants for **3** were obtained from a least-squares fit of the setting angles of 28 carefully centered reflections. Intensity data for this compound were collected on a Siemens P4 diffractometer using the ω-2θ scan technique. Data were corrected for Lorentz and polarization effects, but no absorption correction was carried out due to a small absorption coefficient. Compound **2** was examined on a Siemens SMART CCD-detector system equipped with a cryogenic nitrogen cold stream. Cell constants were obtained from a subset of 8192 strong reflections. Data collection was performed by a hemisphere run taking frames at 0.30° in ω. Corrections for Lorentz and polarization effects and a semiempirical absorption correction using the program SADABS[6] were applied. The Siemens ShelXTL[7] software package was

Table 1. Crystallographic Data for $[Ru^{II}_2(L-L)](BPh_4)_4 \cdot 10CH_3CN$ and $[LRuRuRuL](PF_6)_2 \cdot H_2O$

	$[Ru^{II}_2(L-L)](BPh_4)_4 \cdot 10CH_3CN$	$[LRuRuRuL](PF_6)_2 \cdot H_2O$
empirical formula	$C_{194}H_{218}B_4N_{16}Ru_2S_6$	$C_{78}H_{110}F_{12}N_6OP_2Ru_3S_6$
fw	3211.58	1933.23
space group	*C*2/*c*	$P2_1/n$
a, Å	28.734(5)	18.755(3)
b, Å	16.347(3)	22.278(4)
c, Å	37.986(7)	21.920(4)
β, deg	102.35(2)	91.69(3)
V, Å	17430(6)	9155(3)
Z	4	4
T, K	100(2)	293(1)
ρ_{calcd}, g cm^{-3}	1.224	1.403
diffractometer used	Siemens SMART	Siemens P4
no. of data	84 559	12 351
no. of unique data	24 971	11 928
no. of params	1005	914
μ(Mo Kα), cm^{-1}	3.02	7.28
R1[a]	0.0459	0.0842
wR2[b]	0.0966	0.1999

[a] Observation criterion: $I > 2\sigma(I)$. $R1 = \Sigma||F_o| - |F_c||/\Sigma|F_o|$. [b] $wR2 = \Sigma[w(F_o^2 - F_c^2)^2]/\Sigma[w(F_o^2)^2]^{1/2}$ where $w = 1/\sigma^2(F_o^2) + (aP)^2 + bP$; $P = (F_o^2 + 2F_c^2)/3$.

used for solution, refinement, and artwork of the structures. All structures were solved and refined by direct methods and difference Fourier techniques with neutral-atom scattering factors incorporated into the program. All non-hydrogen atoms were refined anisotropically except those of disordered parts of **3**, which were isotropically refined. The rotational disorder of the three tertiary butyl groups in **3** was resolved by split-atom models with occupancies of 0.6 and 0.4. Both hexafluorophospate anions were found to be severely disordered. The positions of four fluoride atoms located on an equatorial plane at P1 were also split with occupancies of 0.57 and 0.43, respectively. Two residual density peaks of the difference map were assigned to water molecules with low occupancies (0.6 and 0.4). The nonbonded distances of these water molecules to the nearest fluoride atoms of the hexafluorophosphate anions are 2.8 Å.

Results

Synthesis and Characterization of Complexes. The reaction of $H_3L \cdot 3HPF_6$, $[Ru^{II}Cl_2(dmso)_4]$, and NEt_3 (1:1:3) in refluxing methanol produced a blue-green precipitate, which was purified by chromatography (Al_2O_3) from a CH_2Cl_2 solution. Blue microcrystals of $[Ru^{III}L]$ (**1**) were obtained in 55% yield, which are air-sensitive even in the solid state and must be stored under an argon atmosphere.

Temperature-dependent susceptibility measurements on a solid sample of **1** established that **1** has an effective magnetic moment of 1.83 μ_B at 290 K which monotonically decreases to 1.70 μ_B at 50 K. This behavior is typical for a low-spin Ru^{III} ion (d^5) in an octahedral environment ($S = {}^1/_2$). The $S = {}^1/_2$ state of **1** was confirmed by its X-band EPR spectrum measured in frozen CH_2Cl_2 solution at 10 K to which an excess (100:1) of diamagnetic $[Ga^{III}L]$ had been added, providing a diamagnetic "host lattice". The axial spectrum obtained (Figure S1 (Supporting Information) was successfully simulated with $g_\perp = 2.35$ and $g_{||} = 1.74$. It has also been possible to measure a 400 MHz ^{1}H NMR spectrum of **1** in $CDCl_3$ solution (see Experimental Section). Eight of nine expected paramagnetically shifted proton signals have been observed in the range δ −18 to +39 ppm in addition to a signal for the *tert*-butyl protons at $\delta = 1.2$. This indicates C_3 symmetry of **1** in solution.

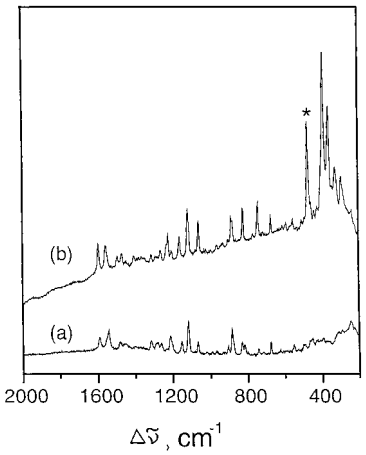

Figure 1. Raman spectra of solid (a) **1** and (b) **2** (KBr disks) (λ = 1064 nm, Nd:YAG laser). The asterisk denotes the ν(S−S) stretching mode at 473 cm^{-1}.

Since **1** is electrochemically readily oxidized by two electrons per mononuclear unit (see below and eq 2), we have carried out a chemical oxidation of **1** in methanol using ferrocenium hexafluorophosphate, $[Fc]PF_6$, as a one-electron oxidant. Thus, from a solution of **1** and $[Fc]PF_6$ (1:2), a *diamagnetic*, microcrystalline red-brown precipitate of $[Ru^{II}_2(L-L)](PF_6)_4$ (**2**) was obtained.

The positive ion electrospray-ionization (ESI) mass spectrum of a CH_3CN solution of **2** displays its 100% peak at *m*/*z* 1959.03 which corresponds to $\{[Ru^{II}_2(L-L)](PF_6)_3\}^+$ (calculated *m*/*z* 1959.04). Simulation of this peak showed the correct isotope pattern. In addition, a peak at *m*/*z* 761.96 (83%) corresponding to $[RuL]^+$ has been identified. This clearly shows that the net two-electron oxidation of **1** produces a dinuclear tetracationic species with exactly twice the mass of **1**.

The 400 MHz ^{1}H NMR spectrum of diamagnetic **2** in CD_3CN solution immediately indicates C_3 symmetry of the tetracation in **2**. Only two doublets for the 12 diastereotopic benzyl protons at $\delta = 4.38$ and 4.81 are observed, in addition to one set of aromatic proton signals for the six pendent arms of the neutral ligand $(L-L)^0$ (see Experimental Section).

Figure 1 shows the Raman spectra of **1** and **2** (KBr disks; Nd:YAG laser; $\lambda = 1064$ nm). In the range 1600−600 cm^{-1}, the vibrational modes observed for the coordinated ligand L^{3-} in **1** and for $(L-L)^0$ in **2** are remarkably similar. Interestingly, in the spectrum of **2**, strong bands at 473, 388, and 360 cm^{-1} are observed which have no counterparts in the spectrum of **1**. We tentatively assign the mode at 473 cm^{-1} to a ν(S−S) stretching frequency of coordinated (L−L), and the bands at 388 and 360 cm^{-1} may be assigned to a ν(Ru−S) stretching mode which in local C_3 symmetry is split into A and E components. The ν(S−S) band at 473 cm^{-1} indicates that the S−S bond of the coordinated disulfide RSSR in (L−L) is rather weak. For example, in Taube's complex,[8] $[\{(NH_3)_5Ru^{III}\}_2(\mu\text{-}S_2)]Br_4$, the ν(S−S) mode has been observed at 519 cm^{-1}, which can be compared to the ν(S−S) stretches for H_2S_2, dialkyl disulfides, and disulfur halides at 509, 495−520, and 510−540 cm^{-1}, respectively.[9] For $[\{CpRu^{III}(PR_3)_2\}_2(\mu\text{-}S_2)]^{2+}$ Rauchfuss et al.[10] have reported a ν(S−S) at 530 cm^{-1}, in agreement with

(6) Sheldrick, G. SADABS, University of Göttingen, 1994.
(7) *ShelXTL V.5*; Siemens Analytical X-ray Instruments, Inc.: Madison, WI, 1994.
(8) Brulet, C. R.; Isied, S. S.; Taube, H. *J. Am. Chem. Soc.* **1973**, *95*, 4758.
(9) Steudel, R. *Angew. Chem.* **1975**, *87*, 683; *Angew. Chem., Int. Ed. Engl.* **1975**, *14*, 655.
(10) Amarasekera, J.; Rauchfuss, T. B.; Wilson, S. R. *Inorg. Chem.* **1987**, *26*, 3328.

a short S−S distance of 1.962(4) Å, which is 2.193(1) Å in Taube's complex. In **2**, the average S−S distance at 2.209(1) Å is slightly longer (see below).

As judged above by ^{1}H NMR spectroscopy, **2** is diamagnetic. A temperature-dependent susceptibility measurement on a solid sample of **2** in the temperature range 4−298 K using a SQUID magnetometer revealed that **2** possesses a significant temperature-independent paramagnetism of $\chi_{TIP} = 868 \times 10^{-6}$ cm^3 mol^{-1} (emu) (0.5% of an $S = {}^1/_2$ impurity). Using the relation $\mu_{eff} = 2.83(\chi_{TIP}T)^{1/2}$, we calculate an effective magnetic moment of 1.44 μ_B at 280 K which decreases to 0.30 μ_B at 10 K.

When a methanol solution of **1** and [Ru^{II}Cl$_2$(dmso)$_4$] (∼1:1) was heated to reflux under an argon atmosphere, a red microcrystalline precipitate of [LRuRuRuL](PF$_6$)$_2$·H$_2$O (**3**) was obtained upon addition of NaPF$_6$, in 30% yield. The ^{1}H NMR spectrum of **3** showed that **3** is diamagnetic and the dication possesses C_3 symmetry (see Experimental Section). The fast-atom bombardement (FAB) mass spectrum displays the 100% molecular ion peak at *m*/*z* 1770.0, which corresponds to the cation {[LRuRuRuL](PF$_6$)}$^+$; further signals are observed at *m*/*z* 1625.4 (75%, [LRuRuRuL]$^+$) and 812.4 (70%, [LRuRuRuL]$^{2+}$). The deep red solution of **3** in CH$_3$CN is air-sensitive; a slow color change to brown is observed.

Crystal Structures. The crystal structures of [Ru$^{II}_2$(L−L)](BPh$_4$)$_4$·10CH$_3$CN and [LRuRuRuL](PF$_6$)$_2$·H$_2$O have been determined by X-ray crystallography at 100 and 298 K, respectively. Table 2 summarizes selected bond distances and angles; Figure 2 shows different views of the tetracation [Ru$^{II}_2$(L−L)]$^{4+}$, and Figure 3, of the dication [LRuRuRuL]$^{2+}$.

Crystals of [Ru$^{II}_2$(L−L)](BPh$_4$)$_4$·10CH$_3$CN consist of well-separated dinuclear cations, tetraphenylborate anions, and acetonitrile molecules of crystallization. The cation posesses crystallographically imposed C_2 symmetry. Each Ru^{II} ion is in an octahedral donor atom environment: *cis*-N$_3$S$_3$Ru. The halves [RuL]$^{2+}$ are connected by three coordinated disulfide groups where the average S−S bond at 2.209(1) Å may be compared with known structures containing coordinated Ru−S−S−Ru moieties with a bridging S_2^{2-} ligand (Table 3).[11−18] Table 4 gives a compilation of structurally characterized disulfide−dimetal complexes where the S−S bond distances are observed in the range 2.036−2.202 Å.[19] The average Ru−S bond length at 2.325(1) Å is rather long. The Ru−N distances (average 2.137 Å) are slightly longer than those in other ruthenium(III) complexes containing a coordinated 1,4,7-triazacyclononane fragment[20] and are typical of low-spin Ru^{II}.

Table 2: Selected Bond Distances (Å) and Angles (deg) of **2** and **3**[a]

	Compound **2**		
Ru1−N1	2.137(2)	Ru1−N2	2.134(2)
Ru1−N3	2.141(2)	Ru1−S3	2.3115(5)
Ru1−S2	2.3180(7)	Ru1−S1	2.3459(6)
S1−S2A	2.2152(7)	S3−S3A	2.198(1)
S2−S1A	2.2151(7)	S1−C9	1.774(2)
S2−C20	1.766(2)	S3−C31	1.759(2)
N2−Ru1−N1	83.06(6)	N2−Ru1−N3	83.25(6)
N1−Ru1−N3	82.51(6)	N2−Ru1−S3	174.50(5)
N1−Ru1−S3	93.61(5)	N3−Ru1−S3	92.00(5)
N2−Ru1−S2	91.73(5)	N1−Ru1−S2	172.97(4)
N3−Ru1−S2	92.22(5)	S3−Ru1−S2	91.21(2)
N2−Ru1−S1	94.11(5)	N1−Ru1−S1	92.85(5)
N3−Ru1−S1	174.89(5)	S3−Ru1−S1	90.42(2)
S2−Ru1−S1	92.23(2)	S3A−S3−Ru1	105.35(2)
S1A−S2−Ru1	107.66(3)	S2A−S1−Ru1	104.78(2)
C20−S2−S1	100.52(7)	C31−S3−S3A	100.62(6)
C9−S1−S2A	101.55(7)	C9−S1−Ru1	113.06(6)
C20−S2−Ru1	113.02(7)	C31−S3−Ru1	113.24(7)
	Compound **3**		
Ru1−Ru2	2.773(2)	Ru1−Ru3	2.778(2)
Ru1−S1	2.439(5)	Ru1−S2	2.377(5)
Ru1−S3	2.371(5)	Ru1−S4	2.395(5)
Ru1−S5	2.388(5)	Ru1−S6	2.373(5)
Ru2−S1	2.347(5)	Ru2−S2	2.320(5)
Ru2−S3	2.312(5)	Ru2−N1	2.13(1)
Ru2−N2	2.16(2)	Ru2−N3	2.15(1)
Ru3−S4	2.327(5)	Ru3−S5	2.314(5)
Ru3−S6	2.308(5)	Ru3−N4	2.13(1)
Ru3−N5	2.13(1)	Ru3−N6	2.16(2)
S1−C9	1.80(2)	S2−C20	1.77(2)
S3−C31	1.79(2)	S4−C59	1.79(2)
S5−C70	1.82(2)	S6−C48	1.82(2)
Ru2−Ru1−Ru3	178.1(1)	S1−Ru1−S2	88.1(2)
S1−Ru1−S3	86.1(2)	S2−Ru1−S3	87.9(2)
S2−Ru1−S4	99.0(2)	S1−Ru1−S5	100.1(2)
S2−Ru1−S5	170.1(2)	S3−Ru1−S5	87.2(2)
S1−Ru1−S6	171.0(2)	S2−Ru1−S6	86.3(2)
S3−Ru1−S6	100.7(2)	S4−Ru1−S6	87.7(2)
S5−Ru1−S6	86.2(2)	S2−Ru2−S3	90.6(2)
S1−Ru2−S2	91.7(2)	S1−Ru2−S3	89.6(2)
S5−Ru3−S6	89.5(2)	S4−Ru3−S5	90.5(2)
S4−Ru3−S6	90.9(2)	Ru1−S1−Ru2	70.8(1)
Ru1−S3−Ru2	72.6(2)	Ru1−S5−Ru3	72.4(1)
Ru1−S6−Ru3	72.8(1)	Ru1−S4−Ru3	72.1(1)
Ru1−S2−Ru2	72.4(1)		

[a] The carbon atoms C9, C31, C70, C20, C48, and C59 are not labeled in Figure 3 (for the sake of clarity). They represent C atoms that are bound to the respective thiolato sulfur atoms S1−S6.

Crystals of [LRuRuRuL](PF$_6$)$_2$·H$_2$O consist of the linear trinuclear dication [LRuRuRuL]$^{2+}$, well-separated PF$_6$ anions, and one water molecule of crystallization. The dication consists of three face-sharing thiolato-bridged octahedra with a central and two terminal ruthenium ions. The stereochemistry of these trinuclear cations, [{LM^1}$_2$M^2]$^{n+}$, has been discussed previously.[2] It has been noted that the stereochemistry of all trinuclear species containing first-row transition metal ions without distinct direct metal−metal bonding between M^1 and M^2 is dominated by the *achiral* stereoisomer $\Delta(\lambda\lambda\lambda)\cdots\Lambda(\delta\delta\delta)$. Λ and Δ represent the configurations of the three six-membered chelate rings M−S−C−C−C−N adopted by the three pendent thiolate arms of L^{3-} at an LM^1 fragment, and $\lambda\lambda\lambda$ (or $\delta\delta\delta$) describes the conformation of the three five-membered chelates M^1−N−C−C−N formed by the 1,4,7-triazacyclononane backbone of coordinated L^{3-}. In trinuclear complexes containing the achiral $\Delta(\lambda\lambda\lambda)\cdots\Lambda(\delta\delta\delta)$ stereoisomer, the six thiolates adopt a stag-

(11) Elder, R. C.; Trkula, M. *Inorg. Chem.* **1977**, *16*, 1048.
(12) Amarasekera, J.; Rauchfuss, T. B.; Rheingold, A. L. *Inorg. Chem.* **1987**, *26*, 2017.
(13) Mizobe, Y.; Hosomizu, M.; Kawabata, J.; Hidai, M. *J. Chem. Soc., Chem. Commun.* **1991**, 1226.
(14) Matsumoto, T.; Matsumoto, K. *Chem. Lett.* **1992**, 559.
(15) Kawano, M.; Hoshino, C.; Matsumoto, K. *Inorg. Chem.* **1992**, *31*, 5158.
(16) Matsumoto, K.; Matsumoto, T.; Kawano, M.; Ohnuki, H.; Shichi, Y.; Hishide, T.; Sato, T. *J. Am. Chem. Soc.* **1996**, *118*, 3597.
(17) Sellmann, D.; Lechner, P.; Knoch, F.; Moll, M. *J. Am. Chem. Soc.* **1992**, *114*, 922.
(18) Schneider, R.; Wieghardt, K.; Nuber, B. *Inorg. Chem.* **1993**, *32*, 4935.
(19) (a) Boorman, P. M.; Kerr, K. A.; Kydd, R. A.; Moynihan, K. J.; Valentine, K. A. *J. Chem. Soc., Dalton Trans.* **1982**, 1401. (b) Bernal, I.; Atwood, J. L.; Calderazzo, F.; Vitali, D. *Isr. J. Chem.* **1977**, *15*, 153. (c) Bernal, I.; Atwood, J. L.; Calderazzo, F.; Vitali, D. *Gazz. Chim. Ital.* **1976**, *106*, 971. (d) Braunwarth, H.; Lau, P.; Huttner, G.; Minelli, M.; Günauer, D.; Zsolnai, L.; Jibril, I.; Evertz, K. *J. Organomet. Chem.* **1991**, *411*, 383.
(20) (a) Geilenkirchen, A.; Neubold, P.; Schneider, R.; Wieghardt, K.; Flörke, U.; Haupt, H.-J.; Nuber, B. *J. Chem. Soc., Dalton Trans.* **1994**, 457. (b) Schneider, R.; Jüstel, T.; Wieghardt, K.; Nuber, B. *Z. Naturforsch.* **1994**, *49B*, 330.

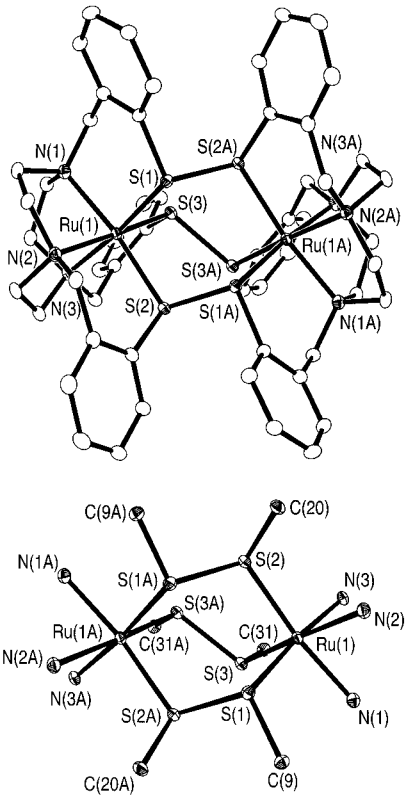

Figure 2. Views of the tetracation in crystals of $[Ru^{II}_2(L-L)](BPh_4)_4 \cdot 10CH_3CN$ (*tert*-butyl groups not shown). Top: view with the crystallographic C_2 axis running perpendicular to the paper plane bisecting the S3−S3A bond. Bottom: view of the core structure of the tetracation.

Table 3. Structural Data for Complexes Containing a Ru−S−S−Ru Moiety

complex	Ru−S, Å	S−S, Å	ref
$[\{Ru^{III}(NH_3)_5\}_2(\mu\text{-}S_2)]Cl_4 \cdot 2H_2O$	2.193 (av)	2.014	9
$[\{CpRu^{III}(PPh_3)_2\}_2(\mu\text{-}S_2)](BF_4)_2$	2.208	1.962	8
1,4-$[\{(MeCp)Ru(PPh_3)\}_2(\mu\text{-}S_2)_2]$	2.295 (av)	2.046	10
$[\{(C_5Me_5)Ru\}_2(\mu\text{-}SR)_2(\mu\text{-}S_2)]$	2.212 (av)	2.008	11
$[\{RuCl(P(OMe)_3)_2\}_2(\mu\text{-}Cl)_2(\mu\text{-}S_2)]$	2.202 (av)	1.971	12, 14
$[\{RuCl(TMP)_2\}_2(\mu\text{-}Cl)(\mu\text{-}N_2H_4)(\mu\text{-}S_2)]$	2.266, 2.296	2.002	13
$[\{Ru(PPh_3)\text{“}S_4\text{”}\}_2(\mu\text{-}S_2)]$	2.357	1.991	15
$[\{LRu(acac)\}_2(\mu\text{-}S_2)](PF_6)_2$	1.989	2.202	16

gered configuration as shown in Figure 3 (bottom left). In contrast, in crystals of **3**, the enantiomers $\Delta(\lambda\lambda\lambda)\cdots\Delta(\lambda\lambda\lambda)$ and $\Lambda(\delta\delta\delta)\cdots\Lambda(\delta\delta\delta)$ are present in equal amounts, since **3** crystallizes in the centrosymmetric space group $P2_1/n$. The configuration of the six thiolates is now eclipsed as depicted in Figure 3 (bottom right). In the achiral $\Delta(\lambda\lambda\lambda)\cdots\Lambda(\delta\delta\delta)$ form, the planes of phenyl rings of one LM^1 fragment are oriented perpendicularly with respect to the same planes of the second LM^1 fragment. In the $\Delta(\lambda\lambda\lambda)\cdots\Delta(\lambda\lambda\lambda)$ isomer (or its enantiomer), these planes are coplanar and the centeroid-to-centeroid distance is 3.92 Å in **3**. The Ru−Ru distance in **3** at 2.775(2) Å is the shortest in all trinuclear species of the above type investigated to date. We speculate that this Ru−Ru bond enforces the observed configuration of the dication.

The two terminal Ru ions have local C_3 (or C_{3v}) symmetry (*cis*-N_3S_3 donor set) whereas the central Ru ion is in a distorted octahedral environment comprising six bridging sulfur atoms. The Ru−N bond distances are very similar to those in **2**. The Ru−S distances of the terminal Ru ions are slightly shorter, at an average 2.321(6) Å, than those of the central ion, at 2.390-

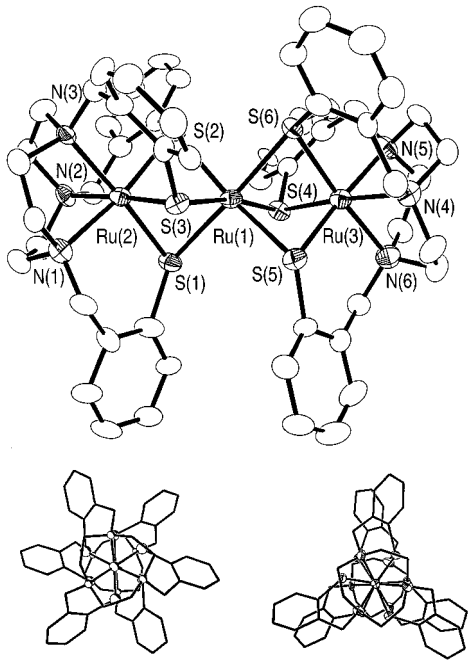

Figure 3. Views of the dication $[LRuRuRuL]^{2+}$ in crystals of **3** (*tert*-butyl groups and Ru−Ru bonds not shown). Bottom left: view down the M···M···M 3-fold axis of achiral cations described in ref 2 with a $\Delta(\lambda\lambda\lambda)\cdots\Lambda(\delta\delta\delta)$ configuration at the terminal metal ions. Bottom right: view of the chiral dication in **3** down the Ru···Ru···Ru axis with a $\Delta(\lambda\lambda\lambda)\cdots\Delta(\lambda\lambda\lambda)$ (or $\Lambda(\delta\delta\delta)\cdots\Lambda(\delta\delta\delta)$) configuration at the two terminal Ru ions.

Table 4. S−S Bond Distances in Selected μ-Disulfide Complexes

complex	S−S, Å	ref
$[\{Cu^{I}I\}_2(\mu\text{-}Et_2S_2)]$	2.063(5)	19a
$[\{Re(CO)_3\}_2(\mu\text{-}Br)_2(\mu\text{-}(CH_3)_2S_2)]$	2.115	19b
$[\{Re(CO)_3\}_2(\mu\text{-}Br)_2(\mu\text{-}Ph_2S_2)]$	2.140	19c
$[\{CpMn(CO)_2\}_2(\mu\text{-}C_3H_6S_2)]$	2.202	19d

Table 5. Structural Data for Complexes Containing a $Ru(\mu\text{-}SR)_3Ru$ Core

complex	Ru−S, Å	Ru−Ru, Å	Ru−S−R, deg	ref
$[\{Cp^*Ru\}_2(\mu\text{-}SPh)_3]Cl$	2.346 (av)	2.630	68.2 (av)	21, 22
$[\{Cp^*Ru\}_2(\mu\text{-}S\text{-}i\text{-}Pr)_3]$	2.388 (av)	2.968	76.6 (av)	23
$[\{(Me_6C_6)Ru^{II}\}_2(\mu\text{-}SPh)_3]Cl \cdot 2CHCl_3$	2.404 (av)	3.354	88.5 (av)	24

(6) Å. As noted above, the most salient feature of the present structure a relatively short Ru···Ru distance at 2.775(2) Å. In conjunction with the fact that **3** is diamagnetic, we feel that direct Ru−Ru metal−metal bonding is occurring in **3**.

Table 5 gives a compilation of structural data for complexes containing a $Ru_2(\mu\text{-}SR)_3$ core.[21−24] When both metal centers possess the formal oxidation state +II, there is no direct Ru··· Ru bond possible and, consequently, the Ru···Ru distance is long at 3.354 Å and the average Ru−S−Ru bond angle is 88.5°.[24] In formally $Ru^{II}Ru^{III}$ mixed-valent species, a Ru−Ru bond of bond order 0.5 may be formed, which decreases the Ru···Ru distance to 2.968 Å and the Ru−S−Ru angle to 76.6°.[23] Finally, when both Ru ions have formally a +III oxidation level,

(21) Hidai, M.; Imagawa, K.; Cheng, G.; Mizobe, Y.; Wakatsuki, Y.; Yamazaki, H. *Chem. Lett.* **1986**, 1299.
(22) Dev, S.; Imagawa, K.; Mizobe, Y.; Cheng, G.; Wakatsuki, Y.; Yamasaki, H.; Hidai, M. *Organometallics* **1989**, *8*, 1232.
(23) Dev, S.; Mizobe, Y.; Hidai, M. *Inorg. Chem.* **1990**, *29*, 4797.
(24) Schacht, H. T.; Haltiwanger, R. C.; Rakowski Du Bois, M. *Inorg. Chem.* **1992**, *31*, 1728.

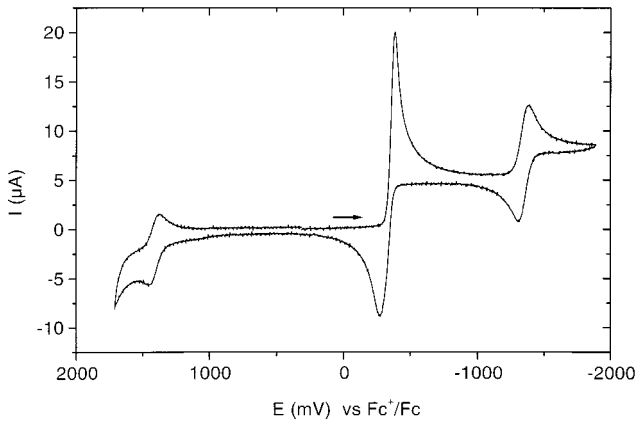

Figure 4. Cyclic voltammogram of **1** ($\sim 10^{-3}$ M) in CH_3CN at 22 °C (0.10 M $[TBA]PF_6$, with a glassy carbon working electrode, an Ag/$AgNO_3$ reference electrode, and a scan rate of 100 mV s^{-1}). That of **2** is identical.

a Ru−Ru single bond is formed (Ru−Ru 2.630 Å; Ru−S−Ru 68.2°).[21,22] Therefore, the Ru···Ru distance at 2.775 Å in **3** is indicative of a metal−metal bond with a formal bond order of 0.5.

Electro- and Spectroelectrochemistry. The electro- and spectroelectrochemistry of **1**−**3** have been studied in depth in acetonitrile solutions containing 0.10 M $[TBA]PF_6$ as the supporting electrolyte. Ferrocene (Fc) was added as internal standard; all potentials are referenced in volts vs the Fc^+/Fc couple.

Figure 4 shows the cyclic voltammogram of **1** at 22 °C. Interestingly, that of **2** is identical under the same conditions. This is a surprising result considering that **1** is a mononuclear Ru^{III}- and **2** is a dinuclear Ru^{II}-containing species. This result immediately implies that **1** and **2** must be electrochemically interconvertible. This interconversion takes place at the electron-transfer wave centered at −0.33 V as was judged from controlled-potential coulometry of **1** at +0.30 V, where **1** is oxidized by *two* electrons per Ru center. In contrast, **2** is *reduced* by four electrons per dinuclear unit at −0.6 V, eq 3. Electronic

$$2\,\mathbf{1} \rightleftharpoons \mathbf{2} + 4e^- \qquad (3)$$

spectra recorded in situ during coulometry displayed isosbestic points at 230, 300, 345, and 537 nm during the oxidation of **1** (by two electrons) and at 295, 348, and 505 nm during the one-electron reduction of **1** yielding $[Ru^{II}L]^-$. The spectra are shown in Figure 5. The final spectrum of the oxidation of **1** is identical to that of genuine sample of **2** in CH_3CN. In addition, CV's recorded at the end of the coulometry experiments were identical to that shown in Figure 4. Table 6 summarizes the electronic spectra of **1**, **2**, and $[Ru^{II}L]^-$. The intense absorptions at 565 and 680 nm of **1** are assigned to thiolato-to-metal charge-transfer bands; they are absent in the spectra of **2** and $[Ru^{II}L]^-$. A similar spectrum has been reported for $[Fe^{III}L]$ (651 nm ($\epsilon = 6.11 \times 10^3$ M^{-1} cm^{-1} and 775 nm ($\epsilon = 4.52 \times 10^3$ M^{-1} cm^{-1})).[1a]

The CV of **1** displays at $E_{1/2} = -1.35$ V a reversible one-electron reduction, and that of **2**, at +1.4 V displays a reversible one-electron oxidation of **2**, generating a mixed-valent $[Ru^{II}$-$Ru^{III}(L-L)]^{3+}$ species. Note that the signal at +1.4 V has approximately half the current height of that of the wave at −1.35 V because the concentration of **2** in the boundary layer is only half that of **1**. These two waves behave as is expected for reversible one-electron-transfer processes; i.e., the peak positions are independent of the scan rate and the peak

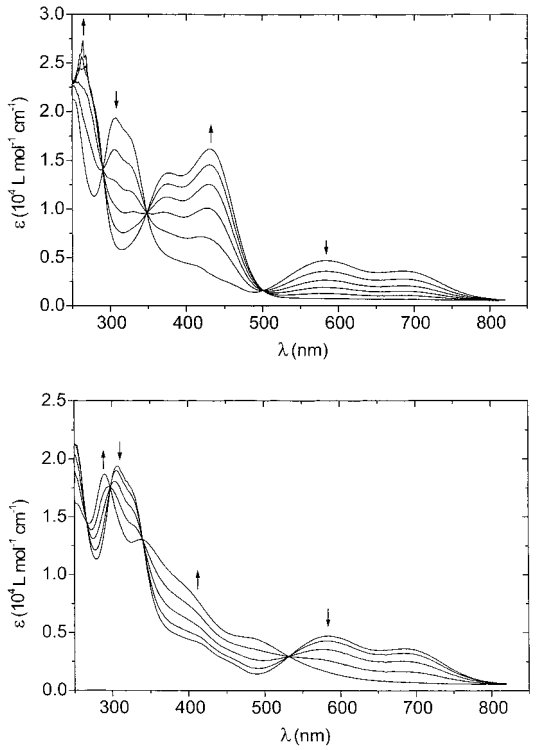

Figure 5. Spectral changes of **1** during a coulometric two-electron oxidation per Ru center (bottom) and a one-electron reduction of **1** at −20 °C (top). (Condition: [**1**] = 10^{-4} M in CH_3CN (0.10 M $[TBA]PF_6$). The final spectra correspond to those of **2** and $[Ru^{II}L]^-$, respectively.

Table 6. Electronic Spectral Data and Magnetic Properties for Complexes **1** − **3** and for the Coulometrically Generated Species

complex	λ_{max}, nm (ϵ, L $mol^{-1}cm^{-1}$)	μ_{eff}, μ_B (293 K)
1	307 (1.9×10^4), 325 sh (1.8×10^4), 410 sh, 590 (4.8×10^3), 690 (3.7×10^3)	1.83
$[LRu^{II}]^-$ [a]	375 (1.4×10^4), 430 (1.6×10^4)	
2	290 (3.7×10^4), 340 (2.6×10^{-4}), 400 sh, 480 sh (9.3×10^3)	dia
3	322 (4.7×10^4), 398 (6.5×10^3), 527 (1.0×10^4), 737 (7.7×10^3), 1072 (7.1×10^3)	dia
$[L_2Ru_3]^{3+}$ [b]	320 (4.8×10^4), 400 sh, 490 (1.5×10^4), 680 (6.0×10^3), ~1300 b (~1.0×10^3)	n.d.

[a] All the electronic spectra were recorded in CH_3CN at 293 K. dia = diamagnetic; n.d. = not determined. [b] Generated by controlled-potential electrolysis at 293 K in CH_3CN (0.10 M $[TBA]PF_6$) solution.

separations, $E^p_{ox} - E^p_{red}$, of ~70 mV are very close to those observed for ferrocene under similar conditions.

Not surprisingly, the wave centered at −0.33 V (i.e., the conversion of **1** to **2** and vice versa) behaves differently since the electrochemical oxidation of **1** (or the reduction of **2**) is accompanied by chemical reactions (i.e., the formation or dissociation of dinuclear **2**).

Thus, we are not dealing with a simple reversible two-electron process of **1** (or **2**) at a potential of −0.33 V as was established by the following experiments. (i) Upon variation of the scan rate (0.02−2.0 V s^{-1}), the current function ($i_p/(SR)^{1/2}$ where i_p is the peak current and SR is the scan rate) was found to be almost constant but the ratio of the current functions of the two waves at −0.32 and −1.3 V is 2 rather than $2^{3/2} = 2.83$. More importantly, the peak positions of the wave at −0.32 V vary with the scan rate where E^p_{ox} is shifted with increasing scan

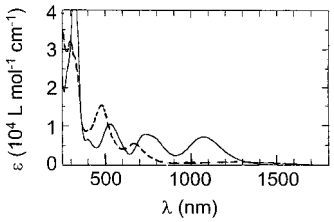

Figure 6. Electronic spectra of **3** (—) and its one-electron-oxidized form $[LRuRuRuL]^{3+}$ (- - -) in CH_3CN.

rate to more positive potentials and E^p_{red} is shifted to more negative ones. The observed shift corresponds to 30 mV per 10-fold increase in scan rate. This behavior is quite typical for a heterogeneous electron transfer followed by a rapid chemical (homogeneous) reaction (EC mechanism). (ii) Figure S2 (Supporting Information) displays cyclic and square-wave voltammograms of **1** and **2** recorded at −20 °C. Again the voltammograms of **1** and **2** are identical as far as the uncomplicated one-electron processes are concerned. However, the oxidative and reductive peaks of the wave at −0.33 V are now well separated. Oxidation of **1** occurs at −0.293 V, and reduction of **2**, at −0.44 V. In the CV, the peaks shift as described above by ∼30 mV per 10-fold increase in scan rate; however, at lower temperatures, the homogeneous chemical reactions are slower and less effective in shifting the two waves toward each other at a given scan rate. Note that, due to convective exchange of species between the diffusion layer and the bulk of the solution at the slow scan rate used in the cyclic voltammetric experiment of Figure S2 (10 mV/s), the peak currents of the reoxidation of **1** and the rereduction of **2** are smaller.

We have attempted to electrochemically obtain kinetic information of the transformation **1**−**2** by performing controlled-potential bulk electrolysis in a thin-layer cell monitoring the spectral changes. Figure S3 (Supporting Information) shows the kinetics of the rapid formation of the CT band of **1** at 584 nm upon reduction of **2** in a 12 μm cell. The formation of **1** proceeds with a half-life of $t_{1/2} = 90$ ms. On this time scale, four electrons per dinuclear **2** have been effectively passed. These half-lives do not reflect the time dependence of a chemical reaction but are governed by diffusion as is revealed by their dependence on the thickness of the layer of the cell (Figure S4 (Supporting Information)). Therefore, at a concentration of **2** of 10^{-3} M, all electrode processes and the dimerization (or break-up thereof) are complete within less than 90 ms. Chronoamperometric experiments with **1** display Cottrell behavior in the time range 0.3 ms−0.3 s on stepping the potential from −0.44 to −0.035 V. This indicates that diffusion is the rate-limiting step for electron transfer in this time domain and, therefore, formation of **2** from **1** is complete within less than 300 μs.

The CV of trinuclear **3** displays in the potential range +0.9 to −1.6 V in CH_3CN (0.10 M $[TBA]PF_6$) three reversible one-electron-transfer waves as shown in Figure S5 (Supporting Information) at redox potentials $E^1_{1/2} = +0.61$ V, $E^2_{1/2} = -0.14$ V, and $E^3_{1/2} = -1.21$ V, which are assigned as in eq 4.

$$[L_2Ru_3]^{3+} \underset{+e}{\overset{-e}{\rightleftharpoons}} [L_2Ru_3]^{2+} \underset{+e}{\overset{-e}{\rightleftharpoons}} [L_2Ru_3]^{+} \qquad (4)$$

The electronic spectra of **3** and its electrochemically generated one-electron-oxidized form $[L_2Ru_3]^{3+}$ are shown in Figure 6. The one-electron-reduced form $[L_2Ru_3]^{+}$ is not stable on the time scale of a coulometric experiment.

(25) Stein, C.; Taube, H. *Inorg. Chem.* **1979**, *18*, 2212.

Discussion

In 1979, Stein and Taube[25] reported the formation of [pentammine(1,2-dithiane)ruthenium(II)]$^{2+}$ by reacting $[(NH_3)_5Ru^{III}-S-(CH_2)_4-SH]^{2+}$ with 1 equiv of the strong *oxidant* cerium(IV). This represents disulfide formation via an oxidatively induced metal-centered reduction. At that time, a Ru(IV) intermediate $[(NH_3)_5Ru^{IV}S(CH_2)_4SH]^{3+}$ had been invoked to explain the intramolecular cyclization to $[(NH_3)_5Ru^{II}$(1,2-dithiane)$]^{2+}$.

In contrast, in the earlier work by Sullivan et al.[26] coordinated thiyl radicals were invoked in a similar "reaction of 1 equiv of oxidant with a coordinated thiol to yield a coordinated disulfide via a radical ion dimer intermediate and induced electron transfer".

The chemical and electrochemical oxidation of mononuclear **1** generating the dinuclear coordinated tris(disulfide) **2** can mechanistically be rationalized following these authors. We propose a one-electron oxidation of **1** yielding a monocation $[RuL]^+$ which can either be formulated as a tris(thiophenolato)-ruthenium(IV) species or, more likely, a Ru^{III} species containing one coordinated thiyl radical and two thiophenolato pendent arms. This radical reacts very rapidly with a neutral $[Ru^{III}L]$ species with formation of a twice Ru^{III}-coordinated disulfide radical anion $[R-S\dot{-}S-R]^{\bullet-}$. Such anions are known to be strong one-electron reductants.[27] Intramolecular one-electron reduction of one Ru^{III} ion to Ru^{II} would generate a dinuclear disulfide-bridged $Ru^{II}Ru^{III}$ species. The second disulfide bridge could form completely analogously. External one-electron oxidation would again form a thiyl radical which could attack—now intramolecularly—a thiolate at the other Ru ion with formation of another $[R-S\dot{-}S-R]^{\bullet-}$ radical anion. Intramolecular electron transfer generates the second Ru^{II} ion and the second disulfide bridge. In the last steps, two electrons (one from each remaining thiolate) must be removed by external oxidants (or an electrode).

Similar reactions of mercapto carboxylic acids with aqueous iron(III) have been kinetically investigated by Sisley and Jordan.[28] The formation of the corresponding disulfide and iron(II) has been observed, and the rapid reaction between a thiyl radical species with its sulfide generating a disulfide radical anion with subsequent intramolecular reduction of iron(III) to iron(II) and disulfide formation has been proposed. On the other hand, we note that Tripathi et al.[29] failed to observe the $[PhSSPh]^{\bullet-}$ species using resonance Raman spectroscopy in aqueous solution containing the $Ph-S^-$ anion and its pulse radiolytically generated phenyl thiyl radical $PhS^{\bullet}$.

Trinuclear ruthenium clusters consisting of a linear array of face-sharing octahedra have been structurally studied in detail by Cotton and co-workers.[30−33] (See Table 7.) Thus complexes containing formally two Ru^{III} ions and one Ru^{II} center ("Ru_3^{8+}") and two Ru^{II} and one Ru^{III} ("Ru_3^{7+}") as well as "Ru_3^{9+}" containing three Ru^{III} ions have been studied whereas a "Ru_3^{6+}"

(26) Woods, M.; Karbwang, J.; Sullivan, J. C.; Deutsch, E. *Inorg. Chem.* **1976**, *15*, 1678.
(27) (a) Surdhar, P. S.; Armstrong, D. A. *J. Phys. Chem.* **1986**, *90*, 5915. (b) Surdhar, P. S.; Armstrong, D. A. *J. Phys. Chem.* **1987**, *91*, 6532.
(28) Sisley, M. J.; Jordan, R. B. *Inorg. Chem.* **1995**, *34*, 6015 and references therein.
(29) Tripathi, G. N. R.; Sun, Q.; Armstrong, D. A.; Chipman, D. N.; Schuler, R. H. *J. Phys. Chem.* **1992**, *96*, 5345.
(30) (a) Bino, A.; Cotton, F. A. *J. Am. Chem. Soc.* **1980**, *102*, 608. (b) Bursten, B. E.; Cotton, F. A.; Fang, A. *Inorg. Chem.* **1983**, *22*, 2127.
(31) Cotton, F. A.; Matusz, M.; Torralba, R. C. *Inorg. Chem.* **1989**, *28*, 1516.
(32) Cotton, F. A.; Torralba, R. C. *Inorg. Chem.* **1991**, *30*, 3293.
(33) Cotton, F. A.; Torralba, R. C. *Inorg. Chem.* **1991**, *30*, 4386.

Table 7. Comparison of Structural Data for Linear Trinuclear Ruthenium Complexes

complex	"Ru_3^{n+}" $n+$	av Ru−Ru, Å	formal Ru−Ru BO	ref
$[Ru_3Cl_8(PEt_3)_4][SbF_6]$	9+	2.91	0.5	32
$[Ru_3Cl_{12}]^{4-}$	8+	2.805	0.5	30
$[Ru_3Cl_8(PR_3)_4]$	8+	2.845	0.5	31
3	8+	2.775	0.5	this work
$[Ru_3Cl_6(PR_3)_6]^+$	7+	3.085	0.25	33

species containing three Ru^{II} ions has to date not been characterized. Complex **3** belongs to the "Ru_3^{8+}" type, but its one-electron-*oxidized* form is a "Ru_3^{9+}" species whereas its one-electron-*reduced* analogue is of the type "Ru_3^{7+}".

The types $n = 9, 8, 7$ have been shown to contain weak Ru−Ru bonds. The formation of three-center MOs by overlap of metal t_{2g} orbitals having lobes along the 3-fold symmetry axis yields a bonding σ_b, a nonbonding σ_n, and an antibonding σ_a molecular orbital.[30] In "Ru_3^{9+}" species, there are three electrons to occupy these MOs, $\sigma_b^2\sigma_n^1$; in "Ru_3^{8+}" there are four electrons, $\sigma_b^2\sigma_n^2$; in "Ru_3^{7+}", there are five electrons, $\sigma_b^2\sigma_n^2\sigma_a^1$; and in "$Ru_3^{6+}$", there are six core electrons, $\sigma_b^2\sigma_n^2\sigma_a^2$. This simple qualitative MO scheme correctly accounts for the observed trend in Ru−Ru bond lengths and predicts the observed electronic ground state which is $S = {}^1/_2$ for "Ru_3^{9+}" and "Ru_3^{7+}" whereas "Ru_3^{8+}" and "Ru_3^{6+}" species are diamagnetic ($S = 0$). The species "$Ru_3^{9+,8+}$" both have a formal Ru−Ru bond order of 0.5, and consequently, the Ru−Ru bond lengths are observed in the narrow range of 2.775 in **3** to 2.91 in $[Ru_3Cl_8(PEt_3)_4][SbF_6]$. In "$Ru_3^{7+}$" species, a σ_a MO is occupied by an electron and the formal BO decreases to 0.25 whereupon the Ru−Ru distance increases to 3.085 Å.[33] For "Ru_3^{6+}" species, the BO drops to zero, which should be accompanied by a further increase of the Ru···u distances.

Acknowledgment. We thank the Fonds der Chemischen Industrie for financial support. B.A. is grateful to the Ministry of Education and Culture of Spain for a fellowship.

Supporting Information Available: Figures S1−S7, showing an EPR spectrum of **1**, square-wave and cyclic voltammograms of **1** and **2**, the time dependence of the electron flow for **2**, the cuolometry of **2**, a cyclic voltammogram of **3**, and additional structural diagrams, and X-ray crystallographic files, in CIF format, for **2** and **3**. This material is available free of charge via the Internet at http://pubs.acs.org.

IC9906297